Selective acetylation of amorphous region of poly(vinyl alcohol) in supercritical carbon dioxide

Matsumoto, Takuya ; Yorifuji, Miyabi ; Hori, Ryohei ; Hara, Mitsuo ; Yamada, L. Norifumi ; Seto, Hideki ; Nishino, Takashi

(Citation)
Polymer Journal,55(12):1287-1293

(Issue Date)
2023-08-23

(Resource Type)
journal article

(Version)
Accepted Manuscript

Selective Acetylation of Amorphous Region of Poly(vinyl alcohol) in Supercritical Carbon Dioxide

Takuya Matsumoto[a*], *Miyabi Yorifuji*[a], *Ryohei Hori*[a], *Mitsuo Hara*[b], *Norifumi L. Yamada*[c], *Hideki Seto*[c], *and Takashi Nishino*[a*]

[a] Department of Chemical Science and Engineering, Graduate School of Engineering, Kobe University, Rokko, Nada, Kobe 657-8501, Japan

[b] Department of Molecular and Macromolecular Chemistry, Graduate School of Engineering, Nagoya University, Furo-cho, Chikusa-ku, Nagoya 464-8603, Japan

[c] Institute of Materials Structure Science, High Energy Accelerator Research Organization, 203-1 Shirakata, Tokai, Ibaraki 319-1106, Japan

Key Word: Supercritical Carbon Dioxide, Poly(vinyl alcohol), Acetylated Poly(vinyl alcohol), Post-functionalization, Hierarchical Structure

ABSTRACT

The post-functionalization of poly(vinyl alcohol) (PVA) with a hierarchical structure has been challenging because conventional polymer functionalization reactions are performed in homogeneous solution states. In this study, the selective functionalization of PVA was achieved in supercritical carbon dioxide (*sc*-CO_2) through acetylation in the amorphous region only, and not in the crystalline region. The crystalline region of PVA was retained in the amorphous-selective acetylated PVA synthesized in *sc*-CO_2. In addition, the oriented structure of the PVA crystallites was maintained even after acetylation of the drawn PVA film in *sc*-CO_2. Moisture adsorption affected the crystalline structure of the PVA acetylated in *sc*-CO_2. The acetylated PVA synthesized in *sc*-CO_2 included a larger number of water molecules under humid conditions, while the increase in thickness was smaller than that of randomly acetylated PVA. This reason was the rigid crystalline structure and the sequential hydrophilic PVA units in the PVA acetylated in *sc*-CO_2.

Introduction

Conventional post-functionalization of polymers progresses in the solution state, where the polymer chains are disentangled and homogeneously dissolved in solvents. Therefore, the polymers are randomly functionalized. For post-functionalization, polymer chains are regarded as a linear chain, and only the degree and distribution of functional groups in the linear chain are focused.[1,2] Controlling the morphology of the functionalized polymers and retaining the hierarchical structure of the precursor polymers have remained challenging.[3,4]

Crystalline polymers possess various hierarchical structures, ranging from chain-folding and growing lamellae to spherulites.[5,6] The size ranges from several nanometers to several millimeters. These hierarchical structures of crystalline polymers contribute significantly to the material performance, such as mechanical properties, thermal properties, and gas permeability.[7–11] Thus, controlling the higher-order structures of polymer materials is significant for the development of high-performance polymer materials.

However, the higher-order structures of crystalline polymers disappear after functionalization because of the random nature of functionalization. Recently, side-chain crystallization has attracted significant attention for controlling higher-order structures after post-functionalization. For example, poly(acrylate ester)s, poly(methacrylate ester)s, and poly(acryl amide)s with long alkyl chains,[12–18] perfluoroalkyl side chains,[19–24] and oligoethylene glycol side chains[25,26] have been reported. The crystallization of the side chains can control the mechanical properties, surface properties, and bio-affinities of the polymers. However, crystallization of the main chain was not observed in these polymers. Moore and co-workers investigated the post-functionalization of polymers in gel states and also their structural and physical properties. Crystalline polymers such

as syndiotactic polystyrene and poly(ether ether ketone) partially retained their crystalline region even after post-functionalization in gel states.[3,4,27–30]

Our group has previously developed the post-functionalization of poly(vinyl alcohol) (PVA) in film state using supercritical carbon dioxide (*sc*-CO_2). Butyralization of PVA in *sc*-CO_2 endowed different mechanical and adhesion properties in gel and solution states.[31] Unfortunately, through post functionalization, the crystalline region of PVA disappeared and the distinct higher-order structure was destroyed. In this study, we achieved the selective acetylation of PVA in the amorphous region alone in *sc*-CO_2. Interestingly, the highly ordered hierarchical structure, including the crystalline structure and orientation, were maintained post functionalization.

Results and discussion

Acetylation of PVA in the film state was performed in *sc*-CO_2 at 60 °C and 15 MPa[31–33] using a pressure reactor cell (Scheme 1). In this reaction condition, the acetylation in *sc*-CO_2 was progressed with high distribution in the samples and high reproducibility. The acetylated PVA (Ac-PVA*sc*) remained in the film state even after the reaction, and the obtained film was dissolved in dimethyl sulfoxide (DMSO). For comparison, Ac-PVAsoln was obtained by the post-functionalization of PVA with acetyl chloride in the solution state. Hexamethylphosphoric triamide (HMPA) was employed as the solvent in the homogeneous solution reaction because both PVA and poly(vinyl acetate) (PVAc) dissolve in HMPA. The progress of acetylation in *sc*-CO_2 and HMPA solution was investigated by nuclear magnetic resonance (NMR) spectroscopy and Fourier transform infrared (FT-IR) spectroscopy. Peaks from PVA and PVAc were observed in the NMR spectra of Ac-PVA*sc* and Ac-PVAsoln, respectively. The quantitative acetylated degrees

(ADs) of the functionalized PVA samples were calculated to be 33 mol% and 52 mol%, respectively, from their NMR spectra.

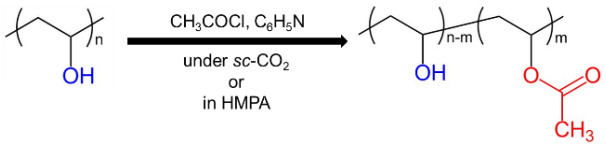

Scheme 1. Acetylation of PVA in *sc*-CO_2 or HMPA solution.

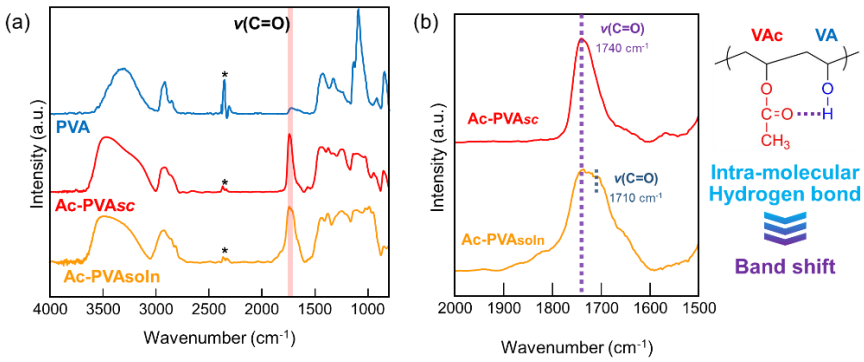

Figure 1. (a) FT-IR spectra of PVA, Ac-PVA*sc* and Ac-PVAsoln, and (b) expanded FT-IR spectra of Ac-PVA*sc* and Ac-PVAsoln at the band of carboxyl groups and schematic image of hydrogen bonding between carboxyl groups and hydroxyl groups.

The FT-IR spectra of PVA, Ac-PVA*sc*, and Ac-PVAsoln are shown in Figure 1a. In the FT-IR spectra of Ac-PVA*sc* and Ac-PVAsoln, absorption bands of the carbonyl groups were observed at approximately 1700 cm^{-1}, indicating that PVA acetylation progressed even in *sc*-CO_2. A sharper absorption band of the carbonyl groups of Ac-PVA*sc* was observed at 1740 cm^{-1} (Figure 1b) relative to that of Ac-PVAsoln. In contrast, Ac-PVAsoln exhibited a broad absorption band of the carbonyl groups and a shoulder at 1710 cm^{-1}. The absorption band at a lower wavenumber was assigned to hydrogen-bonded carbonyl groups. We speculate that the carbonyl groups of Ac-

PVAsoln are hydrogen bonded to the hydroxyl groups of the neighboring monomer units.[34] Because Ac-PVAsoln was randomly acetylated, a large number of acetyl groups were located next to hydroxyl groups. In contrast, a greater number of acetyl groups in Ac-PVA*sc* were isolated from hydrogen bonding interactions. Because *sc*-CO_2 selectively penetrated the amorphous region of PVA, as shown in Figure 2, the amorphous region of PVA was preferentially functionalized in *sc*-CO_2. Therefore, the acetyl groups in Ac-PVAsc were concentrated in the amorphous region, while the remaining crystalline region contained only hydroxyl groups. This selective functionalization resulted in a sharp carbonyl absorption band, without any shoulder. In addition, an absorption band of crystallite region of PVA was observed at around 1140 cm^{-1} in FT-IR spectra of not only PVA but also Ac-PVA*sc*. This data suggested that the crystallite region of PVA was remained through acetylation in *sc*-CO_2.

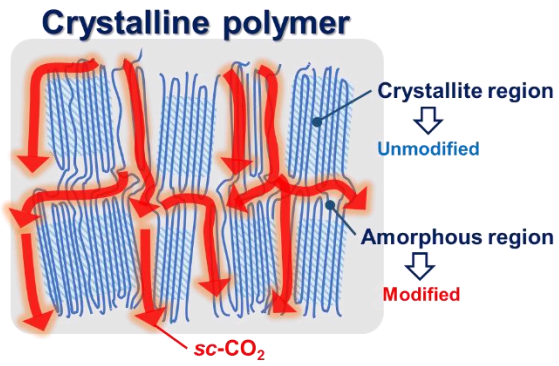

Figure 2. Proposal mechanism of amorphous-selective acetylation of PVA film in *sc*-CO_2.

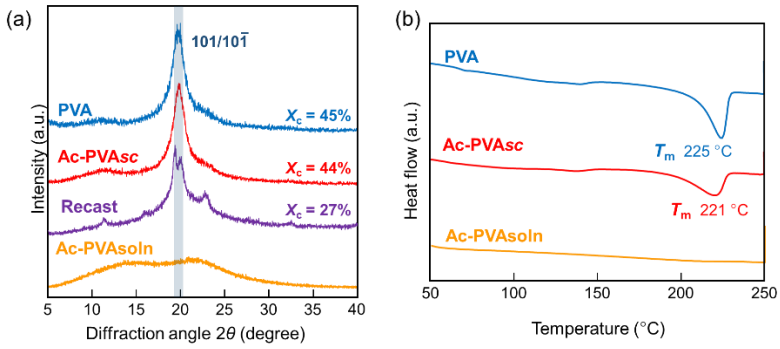

Figure 3. (a) X-ray diffraction profiles and (b) DSC thermograms of PVA, Ac-PVA*sc* and Ac-PVAsoln.

X-ray diffraction measurements were performed to investigate the amorphous-selective acetylation in *sc*-CO_2. The Ac-PVA*sc* film exhibited a 101/10-1 reflection peak of PVA at 19.8°,[35] while Ac-PVAsoln exhibited only an amorphous halo and no diffraction peaks of PVA crystallites (Figure 3a). In only the acetylation in *sc*-CO_2, the crystallite structure, crystallinity X_c, and crystallite size D of PVA were remained. These results supported that acetylation in *sc*-CO_2 progressed in the amorphous region rather than in the crystalline region. After acetylation in *sc*-CO_2, Ac-PVA*sc* was dissolved into DMSO and cast. The DMSO was removed at 200 °C to prepare the recast film. Sharp diffraction peaks of PVA crystallites were observed in the XRD profiles of the recast film. The polymer chains of Ac-PVA*sc* reassembled and formed a crystalline structure after being destroyed upon dissolution into the solvent. However, the crystallinity of the recast film was lower than that of Ac-PVA*sc* because the acetyl groups in the amorphous region and in the folded parts of the crystalline region of Ac-PVA*sc* hindered the reformation and recovery of PVA crystallites in the recast film. The retention of crystallinity in Ac-PVA*sc* and its recovery in the recast film mean that the amorphous-selective acetylation in *sc*-CO_2, and not random acetylation in the solution state, maintained the PVA segments in the crystalline region, promoting

the “blocky” functionalization. This is also the reason for the amorphous-selective penetration of *sc*-CO_2 into the PVA films. These results are consistent with the FT-IR analysis of the isolated carbonyl groups of Ac-PVA*sc*.

The thermal properties of Ac-PVA*sc* and Ac-PVAsoln were investigated by differential scanning calorimetry (DSC). The melting temperature of Ac-PVA*sc* was 221 °C, which was similar to that of unmodified PVA (Figure 3b). No melting temperature was observed in the DSC thermogram of Ac-PVAsoln. These mean that the Ac-PVA*sc* was a crystalline polymer whereas Ac-PVAsoln was an amorphous polymer. This was consistent with the results of the FT-IR and X-ray diffraction analyses. In addition, the crystallinity of Ac-PVA*sc* calculated from the DSC curves and the crystallinity was also remained even after acetylation in *sc*-CO_2. The DSC thermograms of PVA, Ac-PVA*sc*, and Ac-PVAsoln for the cooling and second heating processes are shown in Figure S6–S8. Ac-PVA*sc* also exhibited crystallization temperature at 196 °C, similar to PVA. The observed recrystallization behavior of Ac-PVA*sc* was attributed to the remaining PVA segments through “blocky” functionalization in *sc*-CO_2. However, the DSC curve of Ac-PVAsoln showed a glass transition temperature at 39 °C. The glass transition temperatures at 11 and 45 °C in the DCS thermogram of Ac-PVA*sc* would originat from the side chain and main chain dynamics of PVAc, while that at 87 °C was attributed to PVA (Figure S7).[36] However, the glass transition behaviors of Ac-PVA*sc* were not completely coincident to those of PVA and PVAc. The reason would be that the segment structure in Ac-PVA*sc* were different from those of unmodified PVA and Ac-PVAsoln. These results supported the amorphous-selective post-functionalization of PVA in *sc*-CO_2.

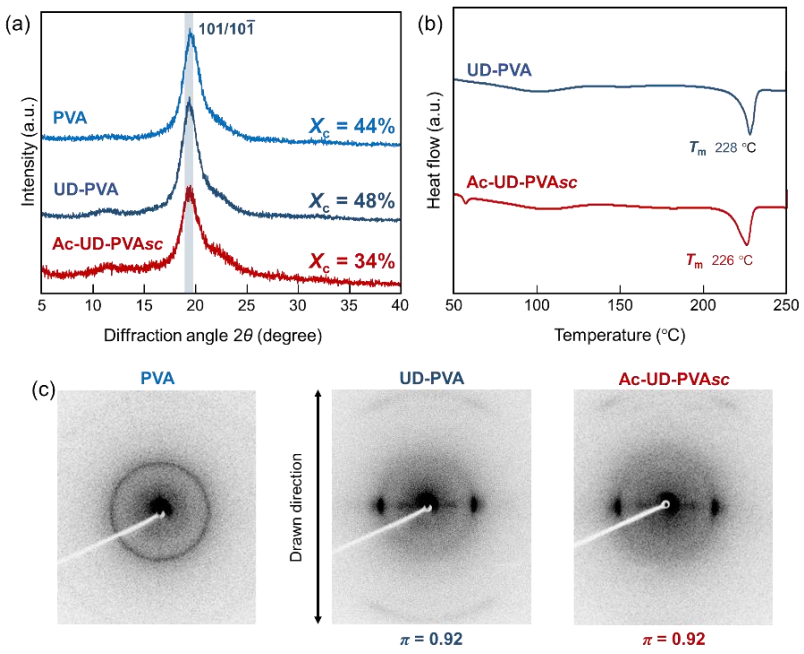

Figure 4. (a) X-ray diffraction profiles, (b) DSC thermograms and (c) X-ray diffraction fiber photograph of undrawn PVA, UD-PVA, and Ac-UD-PVA*sc*.

As mentioned above, the crystalline structure and crystallinity of PVA were maintained after acetylation in *sc*-CO_2. To control the higher-order structure, uniaxially drawn PVA (UD-PVA) was acetylated in *sc*-CO_2 to obtain an Ac-UD-PVA*sc* film. The AD of Ac-UD-PVA*sc* was calculated to be 31 mol% from its ^{1}H NMR spectrum (Figure S9). X-ray diffraction measurements were performed to investigate the structure of Ac-UD-PVA*sc*. The X-ray diffraction profiles and DSC curves revealed almost the same crystalline structure and crystallinity for both Ac-UD-PVA*sc* and UD-PVA (Figure 4a and 4b). X-ray fiber photographs are shown in Figure 4c. The orientation π of more than 90% of the crystallites remained constant even after post-functionalization in *sc*-CO_2. This result suggested that post-functionalization in *sc*-CO_2 progressed almost only in the amorphous region, and that the oriented conformation of crystallite structure of PVA was retained.

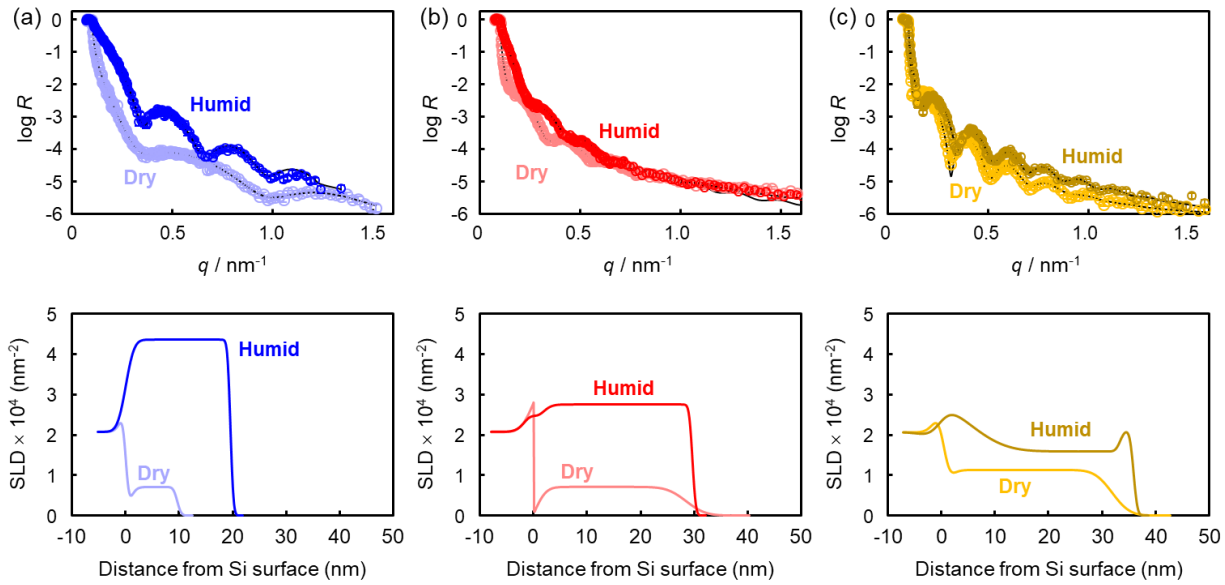

Figure 5. NR profiles (upper) and SLD profiles (bottom) of thin films of (a) PVA, (b) Ac-PVA*sc* and (c) Ac-PVAsoln under dry and humid conditions.

To investigate the moisture absorption behavior of Ac-PVA*sc* functionalized in *sc*-CO_2, neutron reflectivity (NR) measurements of the Ac-PVA*sc* thin films under humid conditions were performed at BL16 SOFIA, MLF, J-PARC reflectometer.[37,38] Thin films of PVA, Ac-PVA*sc*, and Ac-PVAsoln were prepared by spin coating because the smooth thin films with less than 100 nm thickness were indispensable for the NR measurements. The NR profiles and fitting parameters are presented in Figure 5 and Table S3. Kiessig fringes were observed in all NR profiles. The thickness of the PVA thin film under humid conditions increased to approximately twice, relative to that under dry conditions. The reason was that the hydrophilicity of PVA enhanced the absorption of D_2O moisture.[39,40] On the other hand, the thickness of the acetylated PVA thin films, namely the Ac-PVA*sc* and Ac-PVAsoln thin films, was similar under humid and dry conditions. Their relative thicknesses under dry and humid conditions were 104% and 112%, respectively. In

addition, their SLD values under humid conditions were also increased, although the hydrophobic acetyl side chains prevented the adsorption of D_2O, different from the behavior of PVA.

Different changes in the Ac-PVA*sc* and Ac-PVAsoln thin films were observed under dry and humid conditions. The increase in the thickness of the Ac-PVA*sc* film was smaller than that of the Ac-PVAsoln film, whereas the SLD value of the Ac-PVA*sc* film was much larger than that of the Ac-PVAsoln film. Thus, the film thickness and SLD values of the two films followed an opposite trend.

To further investigate these structural changes, the X-ray diffraction measurements were performed under dry and humid conditions; the X-ray diffraction profiles are shown in Figure 6. For PVA, the intensity of the (101/10-1) diffraction peak decreased, and the peak shifted from 19.9° to 19.7° with increasing humidity. It is concluded that this behavior was because water molecules interacted the PVA thin film, including the crystallite region, and increase the distance between the PVA molecular chains in the crystallite cell.[41] In the case of Ac-PVA*sc*, the diffraction peak of the crystallites of Ac-PVA*sc* shifted from 19.9° to 19.7° with increasing humidity. This peak shift in Ac-PVA*sc* was similar to that of PVA crystallites. The inclusion of water molecules in the crystalline region suggested that the hydroxyl groups of the side chains in the crystalline region interacted with the water molecules, and the protons of their hydroxyl groups were exchanged with those of H_2O molecules.[41,42] In contrast, randomly modified Ac-PVAsoln exhibited no crystalline peaks under both dry and humid conditions, as shown in Figure S13.

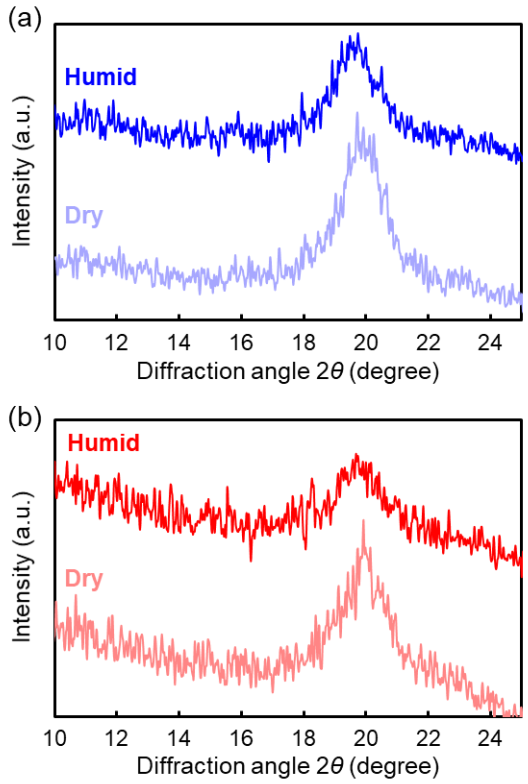

Figure 6. X-ray diffraction profiles of thin films of (a) PVA, and (b) Ac-PVA*sc* under dry and humid conditions.

To understand the behavior of PVA, Ac-PVA*sc* and Ac-PVAsoln under high-humidity conditions, we calculated the volume fraction of water molecules from the SLD values of the results of the NR fitting profiles. The crystalline regions in the PVA and Ac-PVA*sc* thin films interacted with the D_2O molecules. The amorphous regions in all the three samples occupied a large free volume. Therefore, proton-deuterium exchange progressed in both the crystalline and amorphous regions. Because the D_2O vapor flowed and fresh D_2O vapor was provided in the humidity-controlled chamber during the NR measurements, the hydroxyl groups in the samples were deuterated gradually. Therefore, under high-humidity conditions in the NR measurements,

almost all the protons of the hydroxyl groups in the side chains should be exchanged with deuterium.

In this discussion, if all protons of the hydroxyl groups in PVA were exchanged with deuterium, the SLD value of deuterated PVA was estimated to be 2.47×10^{-4} nm^{-2}. Using the SLD values of deuterated PVA and D_2O, the volume fraction of D_2O in the PVA film was estimated to be 48%. The SLD value of deuterated Ac-PVA*sc* including 33% of acetyl groups was calculated to be 1.88×10^{-4} nm^{-2} and the SLD value of Ac-PVA*sc* under humid condition was 2.75×10^{-4} nm^{-2}. Therefore, the volume fraction of water in the Ac-PVA*sc* thin films was 19%. The SLD value of deuterated Ac-PVAsoln was 1.64×10^{-4} nm^{-2} and the bulk layer in the Ac-PVAsoln thin film under humid conditions contained no water molecules. This is because the acetyl groups randomly introduced in Ac-PVAsoln would hamper the penetration of water molecules into the film. Under the conditions of NR measurements, the proton-deuterium exchange at the hydroxyl groups in the samples should not progress completely. If no proton-deuterium exchange occurred, the volume fractions of water in PVA, Ac-PVA*sc*, and Ac-PVAsoln under high humidity conditions would be 65%, 36%, and 9%, respectively. Anyway, Ac-PVA*sc* included a larger volume of water molecules under humid conditions than Ac-PVAsoln. Thus, we concluded that the thickness of the Ac-PVAsc film remained nearly unchanged under humid conditions because the rigid crystallite structure of PVA was retained even after acetylation in *sc*-CO_2.

Conclusions

We selectively acetylated the amorphous region of PVA using *sc*-CO_2. The crystalline structure and orientation of acetylated PVA were retained in *sc*-CO_2, although the randomly acetylated PVA in the solution state possessed only an amorphous region, and not a crystalline region. The crystallinity and orientation before and after acetylation in *sc*-CO_2 were unchanged. In addition, the crystalline structure was formed after recasting because PVA segments were present in the PVA acetylated in *sc*-CO_2. The PVA segments in the PVA acetylated in *sc*-CO_2 absorbed larger amounts of water in the thin film, while the increase in thickness after the absorption of water was smaller than that of randomly acetylated PVA. These results were attributed to the rigid crystalline region of PVA after acetylation in *sc*-CO_2. Our study demonstrates the promising potential of the *block-like* structure of PVA acetylated in *sc*-CO_2.

AUTHOR INFORMATION

Corresponding Author

*(T.N.) E-mail: tnishino@kobe-u.ac.jp

*(T.M.) E-mail: matsumoto0521@person.kobe-u.ac.jp

Author Contributions

The manuscript was written through contributions of all authors. All authors have given approval to the final version of the manuscript.

Acknowledgement

The neutron experiment at the Materials and Life Science Experimental Facility (MLF) of J-PARC was performed under the user program (Proposal No. 2019B0296). This work was

supported by JSPS KAKENHI Grant Number JP22H04546, JP22H04536, JP21K14683, JP20H05222, and JP19H05717.

Notes

The authors declare no competing financial interest.

REFERENCES

1. Goldmann, A. S., Glassner, M., Inglis, A. J. & Barner-Kowollik, C. Post-Functionalization of Polymers via Orthogonal Ligation Chemistry. *Macromol. Rapid Commun.* **34,** 810–849 (2013).

2. Chen, X. & Michinobu, T. Postpolymerization Modification: A Powerful Tool for the Synthesis and Function Tuning of Stimuli-Responsive Polymers. *Macromol. Chem. Phys.* **223,** 2100370 (2022).

3. Fahs, G. B., Benson, S. D. & Moore, R. B. Blocky Sulfonation of Syndiotactic Polystyrene: A Facile Route toward Tailored Ionomer Architecture via Postpolymerization Functionalization in the Gel State. *Macromolecules* **50,** 2387–2396 (2017).

4. Anderson, L. J., Yuan, X., Fahs, G. B. & Moore, R. B. Blocky Ionomers via Sulfonation of Poly(ether ether ketone) in the Semicrystalline Gel State. *Macromolecules* **51,** 6226–6237 (2018).

5. Kishimoto, M., Mita, K., Ogawa, H. & Takenaka, M. Effect of Submicron Structures on the Mechanical Behavior of Polyethylene. *Macromolecules* **53,** 9097–9107 (2020).

6. Baer, E., Hiltner, A. & Keith, H. D. Hierarchical Structure in Polymeric Materials. *Science* **235,** 1015–1022 (1987).

7. Mandelkern, L. The Relation between Structure and Properties of Crystalline Polymers. *Polym. J.* **17,** 337–350 (1985).

8. Tashiro, K. Molecular theory of mechanical properties of crystalline polymers. *Prog. Polym. Sci.* **18,** 377–435 (1993).

9. Oppenlander, G. C. Structure and Properties of Crystalline Polymers . *Science* **159,** 1311–1319 (1968).

10. Tadokoro, H. Structure and properties of crystalline polymers. *Polymer* **25,** 147–164 (1984).

11. Kanehashi, S., Kusakabe, A., Sato, S. & Nagai, K. Analysis of permeability; solubility and diffusivity of carbon dioxide; oxygen; and nitrogen in crystalline and liquid crystalline polymers. *J. Memb. Sci.* **365,** 40–51 (2010).

12. Jordan Jr., E. F. Side-chain crystallinity. V. Heats of fusion and melting temperatures on monomers whose homopolymers have long side chains. *J. Polym. Sci. Part A-1 Polym. Chem.* **10,** 3347–3366 (1972).

13. O'Leary, K. A. & Paul, D. R. Physical properties of poly(n-alkyl acrylate) copolymers. Part 2. Crystalline/non-crystalline combinations. *Polymer* **47,** 1245–1258 (2006).

14. Miho, Y., Hirai, S., Nakano, R., Sekiguchi, H. & Yao, S. Modification of polyethylene using side-chain crystalline block copolymer and evaluation of hydrophilicity. *Polym. J.* **50,** 439–445 (2018).

15. Hirai, S., Ishimoto, S., Obuchi, H. & Yao, S. Improving the adhesion of polyethylene surfaces using Side-Chain crystalline block copolymer. *J. Adhes. Sci. Technol.* **33,** 2567–2578 (2019).

16. Hempel, E., Beiner, M., Huth, H. & Donth, E. Temperature modulated DSC for the multiple glass transition in poly(n-alkyl methacrylates). *Thermochim. Acta* **391,** 219–225 (2002).

17. Wang, X., He, X., Huang, G. & Wu, J. Correlations between alkyl side chain length and dynamic mechanical properties of poly(n-alkyl acrylates) and poly(n-alkyl methacrylates). *Polymer* **53,** 665–672 (2012).

18. Arbe, A., Genix, A.-C., Colmenero, J., Richter, D. & Fouquet, P. Anomalous relaxation of self-assembled alkyl nanodomains in high-order poly(n-alkyl methacrylates). *Soft Matter* **4,** 1792–1795 (2008).

19. Tsibouklis, J., Graham, P., Eaton, P. J., Smith, J. R., Nevell, T. G., Smart, J. D. & Ewen, R. J. Poly(perfluoroalkyl methacrylate) Film Structures: Surface Organization Phenomena, Surface Energy Determinations, and Force of Adhesion Measurements. *Macromolecules* **33,** 8460–8465 (2000).

20. Honda, K., Morita, M., Sakata, O., Sasaki, S. & Takahara, A. Effect of Surface Molecular Aggregation State and Surface Molecular Motion on Wetting Behavior of Water on Poly(fluoroalkyl methacrylate) Thin Films. *Macromolecules* **43,** 454–460 (2010).

21. Yamaguchi, H., Honda, K., Kobayashi, M., Morita, M., Masunaga, H., Sakata, O., Sasaki, S. & Takahara, A. Molecular Aggregation State of Surface-grafted Poly{2-(perfluorooctyl)ethyl acrylate} Thin Film Analyzed by Grazing Incidence X-ray Diffraction. *Polym. J.* **40,** 854–860 (2008).

22. Honda, K., Morita, M., Otsuka, H. & Takahara, A. Molecular Aggregation Structure and Surface Properties of Poly(fluoroalkyl acrylate) Thin Films. *Macromolecules* **38,** 5699–5705 (2005).

23. Volkov, V. V, Platé, N. A., Takahara, A., Kajiyama, T., Amaya, N. & Murata, Y. Aggregation state and mesophase structure of comb-shaped polymers with fluorocarbon side groups. *Polymer* **33,** 1316–1320 (1992).

24. Park, I. J., Lee, S.-B., Choi, C. K. & Kim, K.-J. Surface Properties and Structure of Poly (Perfluoroalkylethyl Methacrylate). *J. Colloid Interface Sci.* **181,** 284–288 (1996).

25. Chua, G. B. H., Roth, P. J., Duong, H. T. T., Davis, T. P. & Lowe, A. B. Synthesis and Thermoresponsive Solution Properties of Poly[oligo(ethylene glycol) (meth)acrylamide]s: Biocompatible PEG Analogues. *Macromolecules* **45,** 1362–1374 (2012).

26. Deng, X., Smeets, N. M. B., Sicard, C., Wang, J., Brennan, J. D., Filipe, C. D. M. & Hoare, T. Poly(oligoethylene glycol methacrylate) Dip-Coating: Turning Cellulose Paper into a Protein-Repellent Platform for Biosensors. *J. Am. Chem. Soc.* **136,** 12852–12855 (2014).

27. Kasprzak, C. R., Anderson, L. J. & Moore, R. B. Tailored sequencing of highly brominated Poly(ether ether ketone) as a means to preserve crystallizability and enhance Tg. *Polymer* **251,** 124918 (2022).

28. Noble, K. F., Troya, D., Talley, S. J., Ilavsky, J. & Moore, R. B. High-Resolution Comonomer Sequencing of Blocky Brominated Syndiotactic Polystyrene Copolymers Using 13C NMR Spectroscopy and Computer Simulations. *Macromolecules* **53,** 9539–9552 (2020).

29. Noble, K. F., Noble, A. M., Talley, S. J. & Moore, R. B. Blocky bromination of syndiotactic polystyrene via post-polymerization functionalization in the heterogeneous gel state. *Polym. Chem.* **9,** 5095–5106 (2018).

30. Anderson, L. J. & Moore, R. B. Sulfonation of blocky brominated PEEK to prepare hydrophilic-hydrophobic blocky copolymers for efficient proton conduction. *Solid State Ionics* **336,** 47–56 (2019).

31. Matsumoto, T., Yorifuji, M., Sugiyama, Y. & Nishino, T. Butyralization of poly(vinyl alcohol) under supercritical carbon dioxide for a humidity-resistant adhesive to glass substrates. *Polym. J.* **52,** 1349–1356 (2020).

32. Koytsoumpa, E. I., Bergins, C. & Kakaras, E. The CO2 economy: Review of CO2 capture and reuse technologies. *J. Supercrit. Fluids* **132,** 3–16 (2018).

33. Nishino, T., Kotera, M., Suetsugu, M., Murakami, H. & Urushihara, Y. Acetylation of plant cellulose fiber in supercritical carbon dioxide. *Polymer* **52,** 830–836 (2011).

34. Rasmussen, R. S. & Brattain, R. R. Infrared Spectra of Some Carboxylic Acid Derivatives. *J. Am. Chem. Soc.* **71,** 1073–1079 (1949).

35. Miyasaka, K. *PVA-Iodine complexes: Formation, structure, and properties BT - Structure in Polymers with Special Properties*. (Springer Berlin Heidelberg, 1993). doi:10.1007/3-540-56579-5_3

36. Sakurada, I. *Polyvinyl Alcohol Fibres*; International Fiber Science and Technology Series; 6; Marcel Dekker, Inc: New York, 1985.

37. Mitamura, K., Yamada, N. L., Sagehashi, H., Torikai, N., Arita, H., Terada, M., Kobayashi, M., Sato, S., Seto, H., Goko, S., Furusaka, M., Oda, T., Hino, M., Jinnai, H. & Takahara, A. Novel neutron reflectometer SOFIA at J-PARC/MLF for in-situ soft-interface characterization. *Polym. J.* **45,** 100–108 (2013).

38. Yamada, N. L., Torikai, N., Mitamura, K., Sagehashi, H., Sato, S., Seto, H., Sugita, T., Goko, S., Furusaka, M., Oda, T., Hino, M., Fujiwara, T., Takahashi, H. & Takahara, A. Design and performance of horizontal-type neutron reflectometer SOFIA at J-PARC/MLF. *Eur. Phys. J. Plus* **126,** 108 (2011).

39. Miyazaki, T., Miyata, N., Yoshida, T., Arima, H., Tsumura, Y., Torikai, N., Aoki, H., Yamamoto, K., Kanaya, T., Kawaguchi, D. & Tanaka, K. Detailed Structural Study on the Poly(vinyl alcohol) Adsorption Layers on a Si Substrate with Solvent Vapor-Induced Swelling. *Langmuir* **36,** 3415–3424 (2020).

40. Miyazaki, T., Miyata, N., Asada, M., Tsumura, Y., Torikai, N., Aoki, H., Yamamoto, K., Kanaya, T., Kawaguchi, D. & Tanaka, K. Elucidation of a Heterogeneous Layered Structure in the Thickness Direction of Poly(vinyl alcohol) Films with Solvent Vapor-Induced Swelling. *Langmuir* **35,** 11099–11107 (2019).

41. Kaji, K. Ph.D. Dissertation, Kyoto University, Kyoto, Japan, 1970. https://doi.org/10.14989/doctor.k997

42. Nitta, I., Seki, S. & Tadokoro, H. Infrared Absorption Spectra of Polyvinyl Alcohol Films Swollen in Water. *Kobunshi ronbunshu* **13,** 45–46 (1956).